Global Scientific JOURNALS

GSJ: Volume 12, Issue 6, June 2024, Online: ISSN 2320-9186
www.globalscientificjournal.com

Raman Spectroscopy Insights: Patterning and Coating Current Impact on Graphitic Thin Film Quality

Churchill B. Agoni[a] **Georgy Fedorov**[a] **Aleksandr Saushin**[a]

[a] Department of Physics and Mathematics, Center of Photonics Sciences, University of Eastern Finland,

Yliopistokatu 7, 80101 Joensuu, Finland.
cagoni@uef.fi

Abstract

In this study, we employ Raman spectroscopy to investigate the structural properties of graphitic thin films fabricated on fused silica substrates. The fabrication process involves nickel catalysis at varying coating currents and two distinct patterning sequences: pre-patterning (lithography before annealing) and post-patterning (lithography after annealing). We analyze the intensity ratios I_D /I_G and I_G /I_{2D}, which serve as indicators of defect density and the number of layers in the graphitic samples. Our findings reveal that both the patterning sequence and the coating current significantly influence these properties. A comparative analysis of pre-patterned and post-patterned samples coated at 100mA, 150mA, and 350mA provides deeper insights into the interplay between the fabrication process and the resulting material properties. This research contributes to the optimization of patterning techniques, potentially enhancing the performance of graphitic materials in various technological applications. The results underscore the importance of meticulous process control in harnessing the full potential of graphitic materials.

Keywords: Annealing, Graphitic film, Lithography, Raman spectroscopy

1. Introduction

Graphitic materials, including graphene and graphite, are celebrated for their exceptional electrical, thermal, and mechanical properties, making them vital in a myriad of advanced technological applications such as electronics, energy storage, and composite materials [1][2]. To optimize these

materials for specific applications, understanding and controlling their structural properties is essential.

Nickel-catalyzed graphitic thin films are created using chemical vapor deposition (CVD). In this process, methane decomposes at high temperatures (~1000°C) on a nickel substrate, leading to the formation of graphitic layers. The nickel catalyzes carbon atom diffusion and precipitation, enabling the growth of single-layer or multi-layer graphene depending on the deposition conditions and thickness of the nickel film [3]

Raman spectroscopy has become an indispensable, non-destructive technique for probing the structural and electronic characteristics of graphitic materials [4]. Key features in the Raman spectra of these materials include the D band (~1350cm^{-1}), the G band (~1580cm^{-1}), and the 2D band (~2700cm^{-1}) [5]. The intensity ratios of these bands, specifically I_D/I_G and I_G/I_{2D}, are crucial indicators of defect density, disorder, and layer thickness in graphitic samples [6].

Patterning techniques are often employed to tailor the properties of graphitic materials. These techniques can be categorized based on the sequence of lithography and annealing processes. In pre-patterned samples, lithography is performed before annealing, potentially influencing the material's structural integrity during subsequent thermal treatment [7]. Conversely, in post-patterned samples, annealing is conducted before lithography, which might affect how the material responds to patterning [8].

This study uses Raman spectroscopy technique to look at how different steps in the making of graphitic samples affect their structure. We're looking at samples that were patterned before and after they were heated (annealed), and coated with different amounts of current (100mA, 150mA, and 350mA).

The goal is to use this information to improve how we make graphitic materials, so they work better in different technologies [10][11].

2. Methods

The substrate (Fused Silica {FS}), utilized in this research, underwent a meticulous cleaning process utilizing a plasma etching machine, operated at its highest power setting for two minutes. A Nickel film was deposited onto the cleaned substrates using the Quorum Q300TT PLUS thermal

evaporator. The apparatus coated a 10*nm thickness of n*ickel (Ni) film on three samples of Fused Silica (FS) substrate each at 100mA, 150mA and 350mA of currents respectively.

2.2 Synthesis of the graphitic thin film on the pre-patterned samples

After cleaning, the substrates were spin-coated with AZnLOF 2070 resist in a 1:4 ratio, at a speed of 2000*rpm* for 60 seconds. Subsequently, the samples were baked for one minute at 110°C. For this research, a GPF file was designed and converted into a job file for the lithographic exposure of the samples using the RAITH VISTEC EBPG 5000+ equipment. The current value for the lithography process was set at 100*nA*.

Following the lithography process, substrates were baked at 110^0C for 60 seconds, immersed in AR300-47 developer solution for 90 seconds, rinsed in water for 30 seconds, and dried with air. With the negative resist, the developer dissolves the unexposed areas, leaving behind the exposed pattern.

The developed samples were placed in the Carbolite CTF CVD reactor whose chamber was evacuated until reaching negligible pressure, followed by the introduction of hydrogen gas (*H*2) at a flow rate of 20 sccm, later adjusted to 5sccm. The samples were then annealed to about 800°C for 60 minutes. After annealing, the chamber pressure rose to 10*mbar* with 20sccm influx of (*H*2), and the system cooled to ambient temperature overnight in a hydrogen atmosphere. Before chamber access, nitrogen gas (*N*2) equalized internal and external pressures until reaching about 850*mbar*.

2.3 Synthesis of the graphitic thin film on the post-patterned samples

The post-patterned samples were subjected to an identical cleaning process, nickel coated at 10*nm* thickness, and spin-coated with same negative resist. However, in contrast to the pre-patterned, these substrates were spin-coated again with a positive resist (AR-P67211 at 2:1) and annealed before the lithography process. Thus, described as post-patterned samples.

3. Results

The Raman spectra of the graphitic films were observed at 514*nm* wavelength with the Renishaw Invia Raman Microscope at 50X objective, powered at 10percent, and exposed for 15seconds. The spectra reveal clear characteristics of D (around 1350cm^{-1}), G (around 1580cm^{-1}), and 2D (around 2700cm^{-1}) peaks in the samples under study. Figures 3.1 and 3.2 show the spectra from these

samples under study while Tables 3.1 and 3.2 present the normalized intensity values and intensity ratios of D to G and G to 2D peaks.

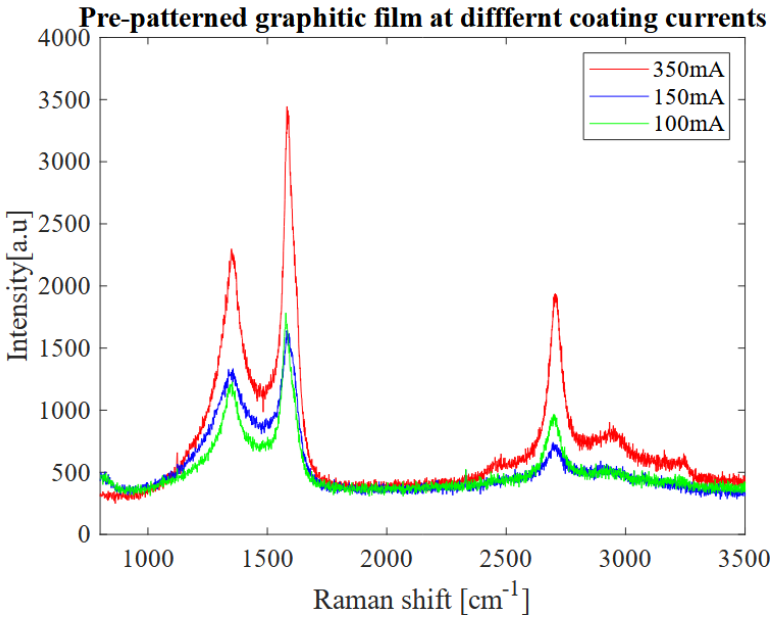

Figure 3.1: The Raman Spectra of nickel-catalyzed pre-patterned graphitic film at 514*nm* laser wavelength for different coating currents.

Table 3.1: Details obtained from the Raman Spectroscopy analysis of pre-patterned graphitic film on fused silica substrates

Intensity values and intensity ratios of pre-patterned graphitic film on fused silica					
Coating current	**Intensity values**			**Intensity ratios**	
	I_D	**I_G**	**I_{2D}**	**I_D/I_G**	**I_{2D}/I_G**
100mA	0.31	0.45	0.24	0.69	0.53
150mA	0.33	0.41	0.19	0.80	0.46
350mA	0.57	0.86	0.48	0.66	0.56

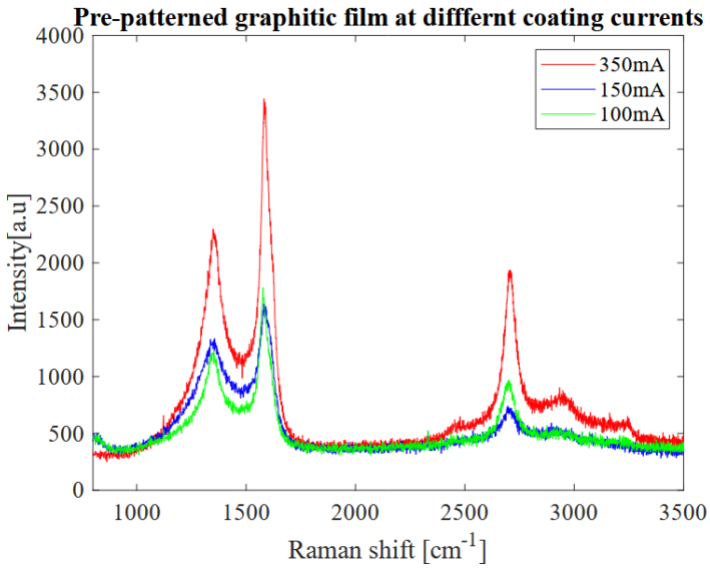

Figure 3.2: The Raman Spectra of nickel catalyzed pre-patterned graphitic film at 514*nm* laser wavelength for different coating currents

Table 3.1: Details obtained from the Raman Spectroscopy analysis of pre-patterned graphitic film on fused silica substrates

Intensity values and intensity ratios of post-patterned graphitic film on fused silica					
Coating current	**Intensity values**			**Intensity ratios**	
	I_D	**I_G**	**I_{2D}**	**I_D/I_G**	**I_{2D}/I_G**
100mA	0.52	0.89	0.60	0.58	0.67
150mA	0.54	0.85	0.44	0.63	0.52
350mA	0.62	0.83	0.35	0.75	0.42

3.2 Discussion

The I_D intensity in the Raman spectrum corresponds to the D-band, which is around 1350cm^{-1} and is indicative of defects, disorder, and the presence of sp^3-hybridized carbon atoms [12][13]. The I_G intensity corresponds to the G-band, around 1580cm^{-1}, associated with the in-plane vibration of sp^2-hybridized carbon atoms [12][13]. A high I_D/I_G ratio indicates a high density of defects such as vacancies, grain boundaries, or functional groups disrupting the sp^2 lattice [14]. This ratio suggests the presence of more sp^3-hybridized carbon atoms, implying structural imperfections [14].

Causes of a high I_D/I_G ratio include aggressive etching or patterning processes that damage the lattice structure, thereby increasing defect density [15][16].

A low I_D/I_G ratio reflects a lower density of defects and higher crystalline quality [14]. This indicates a predominance of sp^2-hybridized carbon atoms with fewer disruptions [14]. Such low ratios are typically observed in well-prepared, high-quality graphitic films [15][16].

The I_{2D} intensity corresponds to the 2D-band, around 2700cm^{-1}, which is a second-order overtone of the D-band and sensitive to the electronic properties of the material [17][18]. The I_G intensity remains associated with the G-band, indicating the presence of sp^2-hybridized carbon atoms [17][18].

A high I_{2D}/I_G ratio indicates fewer layers and high-quality, defect-free graphene. For monolayer graphene, this ratio is typically around 2 or higher [19][20]. This suggests a well-ordered sp^2 lattice with minimal defects and high electronic quality [19][20]. A low I_{2D}/I_G ratio implies multiple layers or increased disorder within the graphitic structure [19][20]. This can indicate the presence of defects such as grain boundaries, vacancies, or other disruptions in the sp^2 lattice [19][20]. Such low ratios are typically observed in thicker films or those with significant structural imperfections [19][20]. Electron-beam lithography amongst other factors influences defect density and I_D/I_G and I_{2D}/I_G ratios in graphitic thin films through exposure, development steps, resist contamination, and beam scattering [15][21].

The Coating Current is also another factor influencing the defect density and I_D/I_G and I_{2D}/I_G ratios. A High current density can lead to rapid deposition and higher defect density, increasing the I_D/I_G ratio [22]. Conversely, a low current density promotes uniform growth with fewer defects, resulting in a lower I_D/I_G ratio [22][23].

In this study, we analyzed the defect intensities in graphitic thin films fabricated on fused silica substrates. The fabrication process involved nickel catalysis and varied coating currents. The defect intensities were assessed using the I_D/I_G and I_{2D}/I_G ratios from the Raman spectra. These ratios are critical indicators of defect density in graphitic materials. A higher I_D/I_G ratio typically suggests a higher density of defects [14].

3.2.1 Pre-Patterned Samples:

At 100mA coating current, the I_D/I_G ratio is 0.69, indicating a moderate level of defects. At 150mA, the I_D/I_G ratio increases to 0.82, suggesting an increase in defect density. At 350mA, the I_D/I_G ratio decreases to 0.66, indicating a decrease in defects with higher coating current.

3.2.2 Post-Patterned Samples:

At 100mA coating current, the I_D/I_G ratio is 0.58, suggesting a moderate level of defects. At 150mA, the I_D/I_G ratio increases to 0.63, indicating an increase in defect density. At 350mA, the I_D/I_G ratio is approximately between 0.70 to 0.80, suggesting a further increase in defects with higher coating current.

4. Conclusion

Both pre-patterned and post-patterned samples show an increase in the I_D/I_G ratio (defect density) with coating current. However, the pre-patterned samples show a decrease in this ratio at 350mA, while the post-patterned samples show an increase. The pre-patterned samples show a higher I_D/I_G ratio at 150mA compared to the post-patterned samples, indicating a higher defect density. However, at 350mA, the post-patterned samples show a higher I_D/I_G ratio, suggesting a higher defect density.

This comparative analysis suggests that the patterning process (pre vs. post) influences how the coating current affects defect formation in the graphitic films. Careful control of the patterning process and coating current is essential to manage the I_D/I_G and I_{2D}/I_G ratios, thereby optimizing the defect density and quality of graphitic thin films for various applications. Understanding and monitoring these ratios through Raman spectroscopy provide valuable insights into the structural and electronic quality of the films The findings from this study provide valuable insights into the fabrication of nickel-catalyzed graphitic thin films. Understanding how the patterning process and coating current affect defect density can guide the optimization of fabrication processes for electronic applications. These findings contribute to the body of knowledge in the field and have potential implications for the development of high-performance electronic devices.

References

[1] R. Saito, G. Dresselhaus, M. S. Dresselhaus, "Physical Properties of Carbon Nanotubes," Imperial College Press, 1998.

[2] A. K. Geim, K. S. Novoselov, "The rise of graphene," *Nature Materials*, vol. 6, pp. 183-191, 2007.

[3] Shuang Chen, Wei Xiong, Yun Shen Zhou, Yong Feng Lu, Xiao Cheng Zeng, "An ab initio study of the nickel-catalyzed transformation of amorphous carbon into graphene in rapid thermal processing", *Nanoscale* **8**, 9746-9755, (2016), DOI: 10.1039/C5NR08614K

[4] A. C. Ferrari, "Raman spectroscopy of graphene and graphite: Disorder, electron-phonon coupling, doping and nonadiabatic effects," *Solid State Communications*, vol. 143, pp. 47-57, 2007.

[5] A. Jorio, M. S. Dresselhaus, R. Saito, G. Dresselhaus, "Raman Spectroscopy in Graphene Related Systems," *Wiley-VCH*, 2011.

[6] C. Casiraghi, A. Hartschuh, E. Lidorikis, et al., "Rayleigh imaging of graphene and graphene layers," *Nano Letters*, vol. 7, pp. 2711-2717, 2007.

[7] L. G. Cançado, A. Jorio, E. H. Martins Ferreira, et al., "Quantifying defects in graphene via Raman spectroscopy at different excitation energies," *Nano Letters*, vol. 11, pp. 3190-3196, 2011.

[8] F. Schwierz, "Graphene transistors," Nature Nanotechnology, vol. 5, pp. 487-496, 2010.

[9] H. Wang, T. Maiyalagan, X. Wang, "Review on Recent Progress in Nitrogen-Doped Graphene: Synthesis, Characterization, and Its Potential Applications," *ACS Catalysis*, vol. 2, pp. 781-794, 2012.

[10] D. C. Wei, Y. Q. Liu, "Controllable Synthesis of Graphene and Its Applications," *Advanced Materials*, vol. 22, pp. 3225-3241, 2010.

[11] A. C. Ferrari, D. M. Basko, "Raman spectroscopy as a versatile tool for studying the properties of graphene," *Nature Nanotechnology*, vol. 8, pp. 235-246, 2013.

[12] Ferrari, A. C., & Robertson, J. (2000). Interpretation of Raman spectra of disordered and amorphous carbon. *Physical Review B*, 61(20), 14095.

[13] Dresselhaus, M. S., Dresselhaus, G., Saito, R., & Jorio, A. (2005). Raman spectroscopy of carbon nanotubes. *Physics Reports*, 409(2), 47-99.

[14] Pimenta, M. A., Dresselhaus, G., Dresselhaus, M. S., Cancado, L. G., Jorio, A., & Saito, R. (2007). Studying disorder in graphite-based systems by Raman spectroscopy. *Physical Chemistry Chemical Physics*, 9(11), 1276-1291.

[15] Novoselov, K. S., Geim, A. K., Morozov, S. V., Jiang, D., Zhang, Y., Dubonos, S. V., ... & Firsov, A. A. (2004). Electric field effect in atomically thin carbon films. *Science*, 306(5696), 666-669.

[16] Ferrari, A. C., Meyer, J. C., Scardaci, V., Casiraghi, C., Lazzeri, M., Mauri, F., ... & Robertson, J. (2006). Raman spectrum of graphene and graphene layers. *Physical Review Letters*, 97(18), 187401.

[17] Malard, L. M., Pimenta, M. A., Dresselhaus, G., & Dresselhaus, M. S. (2009). Raman spectroscopy in graphene. *Physics Reports*, 473(5-6), 51-87.

[18] Graf, D., Molitor, F., Ensslin, K., Stampfer, C., Jungen, A., Hierold, C., & Wirtz, L. (2007). Spatially resolved Raman spectroscopy of single- and few-layer graphene. *Nano Letters*, 7(2), 238-242.

[19] Chen, Z. P., Lin, Y. M., Rooks, M. J., & Avouris, P. (2007). Graphene nano-ribbon electronics. *Physica E: Low-dimensional Systems and Nanostructures*, 40(2), 228-232.

[20] Li, X., Wang, X., Zhang, L., Lee, S., & Dai, H. (2008). Chemically derived, ultrasmooth graphene nanoribbon semiconductors. *Science*, 319(5867), 1229-1232.

[21] Ostrikov, K. (2011). Colloquium: Reactive plasmas as a versatile nanofabrication tool. *Reviews of Modern Physics*, 83(3), 729.

[22] Choi, W., Lahiri, I., Seelaboyina, R., & Kang, Y. S. (2010). Synthesis of graphene and its applications: a review. *Critical Reviews in Solid State and Materials Sciences*, 35(1), 52-71.

[23] Kim, S. M., Huh, J., Kim, H., Song, W., Lee, S. S., Kim, S. H., ... & Choi, J. H. (2013). Defect characterization of graphene grown on copper foil by chemical vapor deposition. *CrystEngComm*, 15(27), 5477-5482.